Available online at www.sciencedirect.com
SCIENCE DIRECT®
Physics of the Earth and Planetary Interiors 143–144 (2004) 93–105
PHYSICS OF THE EARTH AND PLANETARY INTERIORS
www.elsevier.com/locate/pepi

Elasticity and strength of calcium silicate perovskite at lower mantle pressures

Sean R. Shieh [a,*], Thomas S. Duffy [a], Guoyin Shen [b]

[a] *Department of Geosciences, Princeton University, Princeton, NJ 08544, USA*
[b] *GSECARS, University of Chicago, Chicago, IL 60439, USA*

Received 29 November 2002; received in revised form 6 August 2003; accepted 16 October 2003

Abstract

$CaSiO_3$ perovskite was synthesized in a diamond cell and its lattice strain anisotropy was measured under non-hydrostatic compression to conditions corresponding to 61 GPa. Experiments were performed using energy dispersive synchrotron X-ray diffraction in a radial geometry. The equation of state of $CaSiO_3$ perovskite obtained from lattice strains measured at different angles from the loading direction can describe the range of compression curves previously reported under quasi-hydrostatic and non-hydrostatic conditions. The ratio of the differential stress to the shear modulus increases from 0.016(5) to 0.039(4) for $CaSiO_3$ perovskite over pressures from 19 to 61 GPa. In combination with a theoretical prediction for the shear modulus, room-temperature yield strengths are 3–11 GPa for $CaSiO_3$ perovskite over this pressure range. Under the assumption that the effect of the tetragonal distortion is minimal, the elastic constants for $CaSiO_3$ perovskite were recovered. Single-crystal elastic constants of $CaSiO_3$ perovskite are in good agreement with theoretical predictions for the cubic phase. In particular, the elastic anisotropy, S, decreases from 0.0020(7) to 0.0004(2) GPa^{-1} over the 19–61 GPa pressure range. Comparison with theoretical elasticity data provides evidence for possible strength anisotropy.

Keywords: X-ray diffraction; Perovskite; Yield strength; Elasticity; Equation of state

1. Introduction

The single-crystal elastic properties of mantle minerals are essential for interpreting seismic wave velocities and their lateral variations, as well as for understanding seismic anisotropy in the mantle. $CaSiO_3$ perovskite is believed to be an important phase in the Earth's transition zone and lower mantle on the basis of laboratory experiments on expected mantle compositions as well as examination of natural diamond inclusions (Joswig et al., 1995; Fiquet, 2001). Furthermore, it has been suggested as a possible host of large cations such as rare earth elements (REE) and radioactive elements in the deep mantle (Kato et al., 1988). Hence the physical properties of $CaSiO_3$ perovskite are of interest for interpreting seismic observations and understanding the geodynamics and geochemistry of the Earth's deep interior.

The differential stress supported by a sample under loading is a lower bound to the yield strength, and thus, is an important parameter for characterizing mechanical behavior. The low-temperature, high-stress conditions within the non-hydrostatic diamond anvil cell provide insights into rheological behavior in the regime of low-temperature plasticity. The flow law

* Corresponding author. Present address: Department of Earth Sciences, National Cheng Kung University, Taiwan, ROC.
Tel.: +886-6-275-7575x65434; fax: +886-6-274-0285.
E-mail address: sshieh@mail.ncku.edu.tw (S.R. Shieh).

0031-9201/$ – see front matter © 2004 Elsevier B.V. All rights reserved.
doi:10.1016/j.pepi.2003.10.006

under such conditions is governed by the Peierls stress, which is the stress required to move dislocations at 0 K (Evans and Goetze, 1979), and is equivalent to the yield strength. Low-temperature plasticity is important for understanding deformation of the lithosphere (Evans and Goetze, 1979) as well as having technological applications, but relatively little is known about behavior in this regime for silicates. Correlations have been suggested between the room-temperature flow stress and activation energy for high-temperature creep (Karato et al., 1990). In addition to the stress measurements, the texture development observed in radial diffraction experiments can give insights into deformation mechanisms and active slip systems. Perovskites are an important class of compounds and characterizing their mechanical properties across a wide range of conditions is desirable.

The elastic and rheological properties of $CaSiO_3$ perovskite are very poorly understood largely because it is non-quenchable at ambient conditions. Available results on the elastic properties are restricted to analog (Kung et al., 2001) and theoretical studies (Karki and Crain, 1998). Recent studies of the orientation dependence of lattice strains under non-hydrostatic stress in the diamond anvil cell (radial X-ray diffraction method) have shown that constraints on these properties can be obtained for high-symmetry materials (Singh et al., 1998; Kavner and Duffy, 2001a; Merkel et al., 2002; Shieh et al., 2002). Most experimental studies reported that $CaSiO_3$ crystallizes in the cubic structure (Mao et al., 1989; Wang et al., 1996) and first-principles calculations also supported this observation (e.g. Hemley et al., 1987; Sherman, 1993; Wentzcovitch et al., 1995). However, other theoretical calculations favored a tetragonal structure (Chizmeshya et al., 1996; Stixrude et al., 1996) or even lower symmetry (Akber-Knutson et al., 2002; Magyari-Köpe et al., 2002). Calculated energy differences between the proposed phases are sufficiently small that the crystal structure under mantle conditions is uncertain and may be cubic even if a lower symmetry phase is favored at 0 K (Karki and Crain, 1998). Recently, a high-resolution X-ray diffraction study reported the first experimental evidence for the existence of a lower symmetry phase at room temperature through observation of small ($<0.4\%$) splittings in the (2 0 0) and (2 1 1) diffraction lines (Shim et al., 2002). In this paper, we report an in-situ strength and elasticity of $CaSiO_3$ perovskite using energy dispersive radial X-ray diffraction together with lattice strain theory.

2. Experiment

Natural samples from Newburgh, NY were examined by powder X-ray diffraction and confirmed to be wollastonite ($CaSiO_3$). No peaks from any impurity phases were detectable. The powdered sample (grain size ~1–3 μm) was mixed with 10 wt.% Pt, which served as a laser absorber and loaded into a 100-μm Be gasket hole with a pre-indented thickness of ~25 μm in a diamond anvil cell. A small piece of gold foil was placed on the top within 5 μm of the sample center to serve as a positional reference and pressure standard. No pressure-transmitting medium was used. $CaSiO_3$ perovskite was synthesized near 20 GPa by laser heating at temperatures estimated to be less than 1800 K. The sample was heated using the Nd:YLF laser heating set-up at the GSECARS sector of the Advanced Photon Source (Shen et al., 2001). The 20–30 μm diameter laser beam was not scanned across the sample but moved in a step-wise fashion over the whole sample chamber with the laser beam position held fixed for ~2 min at each step. The beam was translated with a step size of ~10 μm in order to ensure overlap of sequential heating spots. The total heating time was more than 30 min. Transformation to the $CaSiO_3$ perovskite phase was confirmed by in situ X-ray diffraction, and no residual diffraction lines attributable to the starting material were observed.

Energy dispersive radial X-ray diffraction experiments were carried out at beamline 13-BM-D of the GSECARS sector of the Advanced Photon Source. All diffraction measurements were made without any further heating after the initial synthesis. The incident X-ray beam was collimated by slits and focused by a pair of Kirkpatrick-Baez mirrors to a size of approximately 12 μm × 11 μm. The beam was directed through the Be gasket, $CaSiO_3$ perovskite, and internal standard. The diffraction signal was detected by a solid-state Ge detector with a fixed angle at $2\theta = 11.998(4)^\circ$, which was calibrated with a gold foil outside the diamond cell. Data were collected only after sufficient time (i.e. 1–2 h) elapsed after each compression step to allow for stress relaxation. The

change in d-spacing over this time interval was generally less than 0.2% and no further detectable change in d-spacing was observed over the measurement time interval. This was verified by recording diffraction patterns for the same orientation at the beginning and end of the measurements at a given loading step.

Spectra were collected as a function of the angle (ψ) between the diffraction plane normal and the diamond cell loading axis over the range from 0 to 90° at approximately 15° intervals. Hydrostatic pressure was determined from data collected at $\psi = 54.7°$ as described below. Lattice spacings were converted to pressures using the equations of state for platinum (Holmes et al., 1989) and/or gold (Shim et al., 2002). In general, although there is some overlap between gold and platinum peaks especially at lower ψ angles and high pressures, we found that the pressures determined from our available gold peaks are consistent with those from platinum ones, i.e. the pressure difference between gold and platinum is of order 1–3 GPa. This also indicates that errors introduced by any platinum dissolution into gold at high temperature are minimal. Aside from pressure determination, however, the gold and platinum diffraction data were not analyzed in detail.

The measured d-spacings were analyzed using the lattice strain theory described by Singh (1993) and Singh et al. (1998). A sample in the diamond anvil cell is characterized by a stress, σ_3, along the diamond cell loading axis, and a radial stress, σ_1. The tensor describing the state of stress in the sample can be divided into hydrostatic and deviatoric components. The d-spacings obtained from X-ray diffraction are then given by

$$d_{\mathrm{m}}(hkl) = d_{\mathrm{p}}(hkl)[1 + (1 - 3\cos^2\psi)Q(hkl)], \quad (1)$$

where d_{m} is the measured d-spacing and d_{p} is the d-spacing under hydrostatic pressure. $Q(h\,k\,l)$ is given by

$$Q(hkl) = \left(\frac{t}{3}\right)\{\alpha[2G_{\mathrm{R}}^{\mathrm{X}}(hkl)]^{-1} + (1-\alpha)(2G_{\mathrm{V}})^{-1}\}, \quad (2)$$

where $G_{\mathrm{R}}^{\mathrm{X}}$ $(h\,k\,l)$ is the X-ray shear modulus under the Reuss (isostress) limit and G_{V} is shear modulus under the Voigt (isostrain) limit (Singh et al., 1998). The parameter, α, which can vary between 0 and 1, is the weighting factor for the relative degree of stress and strain continuity across grain boundaries in the sample. We assumed that the sample was under isostress conditions (Kumazawa, 1969) and hence α is taken to be 1. The effect of varying α will be considered below. According to Eq. (1), when $\psi = 54.7°$, then the quantity $1-3\cos^2\psi = 0$ and the measured d-spacing is equivalent to that under hydrostatic stress. The d-spacing at 54.7° is obtained from linear fits of the measured data to Eq. (1). The differential stress, t, can be obtained from the aggregate shear modulus, G, and the average $Q(h\,k\,l)$ value obtained from all measured reflections by

$$t = 6G\langle Q(hkl)\rangle. \quad (3)$$

Alternatively, the differential stress corresponding to slip along the plane $(h\,k\,l)$ can be obtained if the elastic constants are known through

$$t(hkl) = 6G(hkl)Q(hkl). \quad (4)$$

The differential stress, t, is given by $t = \sigma_3 - \sigma_1 \leq Y = 2\tau$ where τ is the shear strength, and Y is the yield strength. The elastic tensor can also be obtained from the measured lattice strain anisotropy (Singh et al., 1998). For a cubic material, a linear fit to $Q(h\,k\,l)$ versus $3\Gamma(h\,k\,l)$, where $\Gamma(h\,k\,l) = (h^2k^2 + k^2l^2 + l^2h^2)/(h^2 + k^2 + l^2)^2$, yields an intercept, m_0, and slope, m_1, that are related to the elastic compliances for the case where $\alpha = 1$ through

$$m_0 = \frac{t}{3}(S_{11} - S_{12}), \quad (5)$$

$$m_1 = -\frac{t}{3}(S_{11} - S_{12} - 0.5S_{44}), \quad (6)$$

where S_{11}, S_{12}, and S_{44} are the three elastic compliances of a cubic crystal (see Singh et al., 1998 for general expressions that apply to any value of α). Additionally, using the relationship of the bulk modulus, K, to the single-crystal compliances

$$\frac{1}{3K} = S_{11} + 2S_{12}, \quad (7)$$

we are able to calculate the three independent elastic compliances or stiffnesses of a cubic crystal (Singh et al., 1998). The bulk modulus can be obtained from the third-order Birch-Manurghan equation of state and a fit to data at $\psi = 54.7°$. The elastic anisotropy of a

cubic crystal can be described by the Zener anisotropy ratio

$$A = \frac{2C_{44}}{C_{11} - C_{12}} = \frac{2(S_{11} - S_{12})}{S_{44}}. \quad (8)$$

Alternatively, the anisotropy is also commonly described using

$$S = S_{11} - S_{12} - \frac{S_{44}}{2} = \frac{S_{44}(A-1)}{2}. \quad (9)$$

In the case $\alpha = 1$, the Zener anisotropy can be obtained independent of the values of t and G from (5) and (6)

$$A = \frac{m_0}{m_0 + m_1}. \quad (10)$$

3. Results and discussion

Diffraction spectra of $CaSiO_3$ perovskite were measured to conditions corresponding to a hydrostatic pressure up to 61 GPa. With increasing ψ (or decreasing strain) all $CaSiO_3$ peaks shifted to lower energy (higher d-spacing) (Fig. 1). The total shift of the peaks from $\psi = 0$ to 90° is about 0.5–1 keV at the highest pressure of this study. While there is some variation in peak intensity with ψ, these are not systematic and appear to be primarily a result of small sample position changes. More problematic are peak overlaps which affect mainly $CaSiO_3$ perovskite's (1 1 1) line and the (2 0 0) line to a lesser degree.

The full width at half maximum (FWHM) for the $CaSiO_3$ perovskite peaks increases from 0.3–0.5 keV at low pressure to 0.5–1.0 keV at the highest pressures. Consistent with previous energy dispersive diffraction studies, we are unable to observe any splitting or anomalous broadening associated with the low-symmetry distortion found in the recent high-resolution diffraction study (Shim et al., 2002). The FWHM of the (2 0 0), (2 1 1), and (2 2 0) reflections are all similar and slightly larger than that of the (1 1 0) reflection at all pressures. Furthermore, there is no evidence for any systematic angle dependence of the peak width. As a result, we have analyzed these data using the lattice strain equations for the cubic system. This may not produce major errors if the structure remains pseudo-cubic. Indeed, the effect on the compression curve appears to be minor

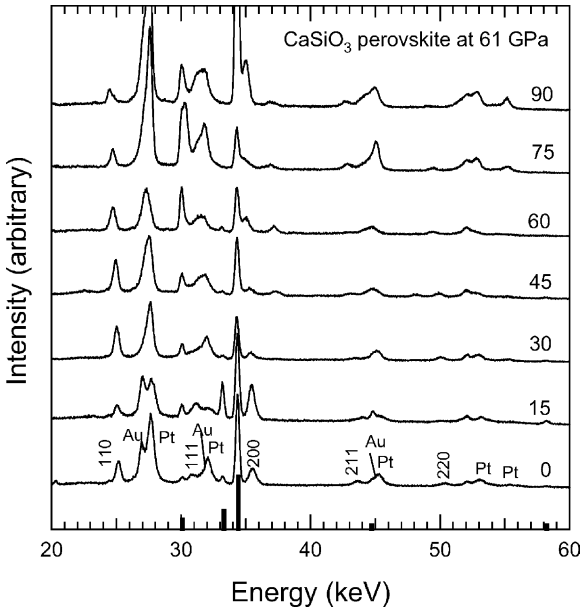

Fig. 1. Energy-dispersive X-ray diffraction spectra of $CaSiO_3$ perovskite obtained at different angles from the loading axis. The value of ψ is indicated next to each spectrum. The pressure, obtained using Eq. (1), is 61 GPa. The sample peaks are labeled with Miller indices. Au is the internal pressure marker, Pt is the laser absorber, and bold vertical lines at the bottom denote Be gasket peaks.

(Shim et al., 2002). However, the effects of the distortion on the elastic tensor and yield strength are difficult to predict: even minor distortions can have major effects near a phase transition boundary (Shieh et al., 2002). Thus, our results for the elastic tensor are only tentative and must be subjected to further examination. We should also note that the symmetry of $CaSiO_3$ perovskite at lower mantle conditions is unknown, and indeed may be cubic (Karki and Crain, 1998). Therefore, the physical properties of cubic $CaSiO_3$ perovskite may well still be of geophysical importance.

In general, our measured d-spacings show a linear relation with $1 - 3\cos^2\psi$, as expected from theory. The value of $Q(h\,k\,l)$ was determined from the slope of the linear fit to Eq. (1) and d_p. Fig. 2 shows plots of d-spacings as a function of $1 - 3\cos^2\psi$ at five different pressures. The (1 1 0), (1 1 1), (2 0 0), (2 1 1), and (2 2 0) lines were generally observable through entire range of our measurements and were used for our data analysis. From the linear fit, we obtained $d_p(h\,k\,l)$

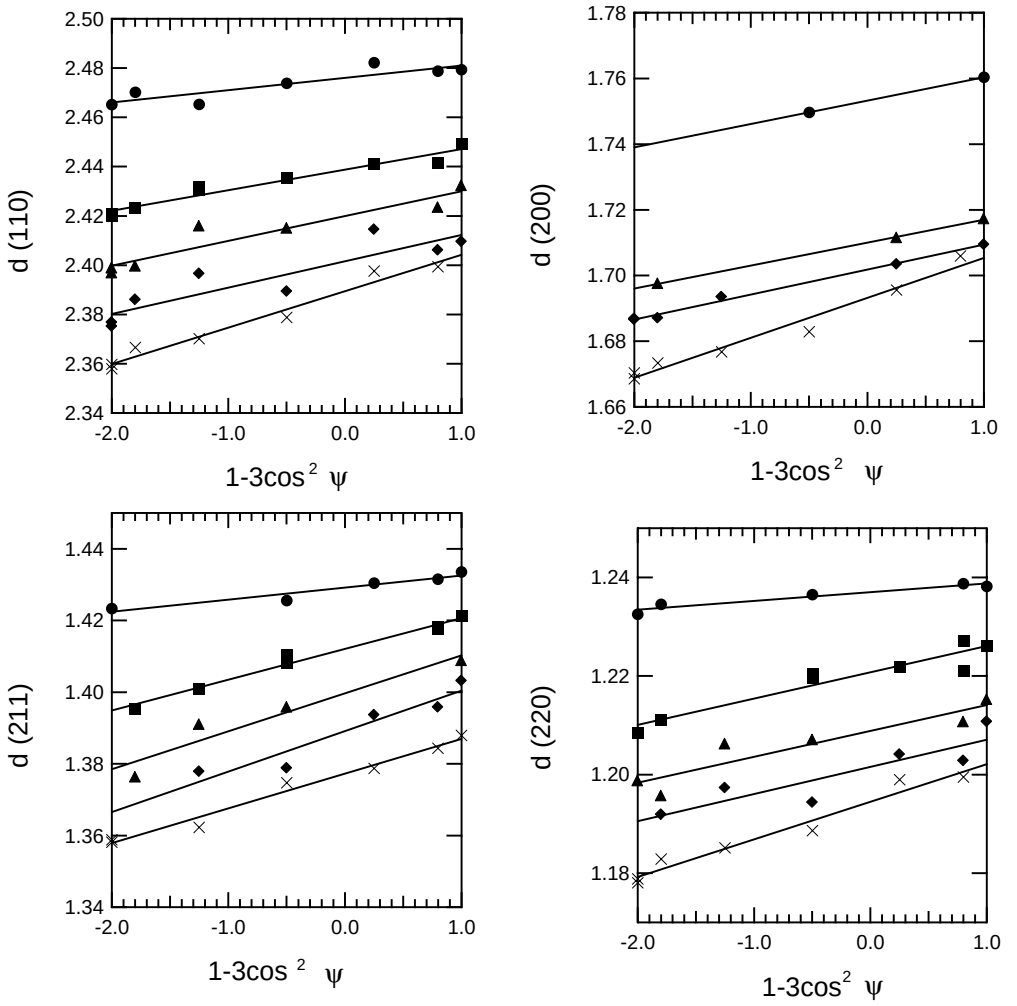

Fig. 2. *d*-spacings as a function of $1-3\cos^2\psi$ for $CaSiO_3$ perovskite at five different pressures. The solid circles are 18.6 GPa, solid squares are 30.6 GPa, solid triangles are 40.6 GPa, solid diamonds are 52.8 GPa, and crosses are 60.8 GPa. The solid lines are linear fits to all the individual ($h\,k\,l$) data sets.

values at $\psi = 54.7^\circ$ or $1-3\cos^2\psi = 0$ and used these data to calculate the compression curve of $CaSiO_3$ perovskite. The corresponding pressure was determined from the *d*-spacing of gold and/or platinum at this angle. Fig. 3 shows a plot of $Q(h\,k\,l)$ as a function of 3Γ. The (2 1 1) line deviates from the linear trend of the data at all pressures. However, there is only a minor effect on the fitted slope and intercept if we removed this line from consideration. The linear fit of $Q(h\,k\,l)$ as function of $3\Gamma(h\,k\,l)$ (Fig. 3) provides two parameters, the intercept, m_0 and the slope, m_1 for resolving single-crystal elastic constants (Eqs. (5) and (6)) as discussed later.

Fig. 4 shows the equation of state determined at angles of 0°, 54.7°, and 90°. In each case, we assumed that the *d*-spacings of both the pressure marker and sample at this angle correspond to the volume compression under hydrostatic stress. While this is only strictly correct at 54.7°, this method facilitates comparison with literature data which typically uses the same assumption in analyzing axial diffraction data even when the stress is not hydrostatic. Data from $\psi =$

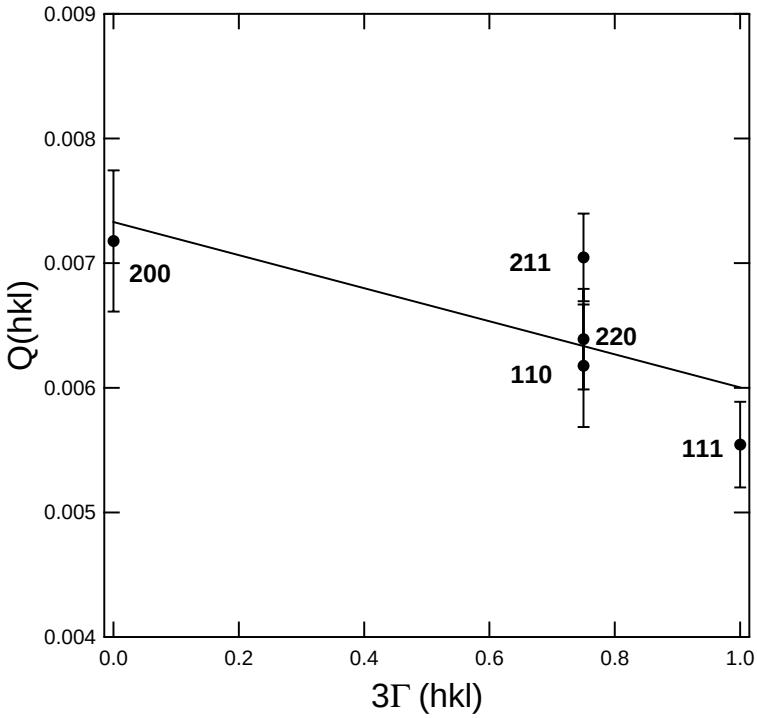

Fig. 3. $Q(h\,k\,l)$ as a function of $3\Gamma(h\,k\,l)$ for $CaSiO_3$ perovskite at 61 GPa.

90° are in excellent agreement with non-hydrostatic compression data reported by Mao et al. (1989) as expected since axial diamond cell experiments are performed near this angle. This is consistent with radial diffraction results for other materials including SiO_2 (Shieh et al., 2002) and rhenium (Duffy et al., 1999). The data from $\psi = 54.7°$ agree best with quasi-hydrostatic data by Shim et al. (2002) and Wang et al. (1996), but are less compressible than earlier data of Shim et al. (2000). A third-order Birch-Manurghan equation of state fit to the data at 54.7° yields a bulk modulus of 246(18) GPa and pressure derivative of 4.5(1.0), which can be compared with the results of Wang et al. (1996) ($K_o = 232(8)$ GPa, $K'_o = 4.8(3)$), Shim et al. (2000) ($K_o = 236(4)$ GPa, $K'_o = 3.9(2)$) and Shim et al. (2002) ($K_o = 255$ GPa, $K'_o = 4$). We note that Shim et al. (2002)'s equation of state data are based on fitting to a tetragonal cell.

The ratio of differential stress to shear modulus, t/G, is directly obtained from the slope of the d-spacing versus $1 - 3\cos^2\psi$ relationship (Eqs. (1) and (3)). In Fig. 5, t/G of $CaSiO_3$ perovskite is found to be in the range of 0.016(5)–0.039(4) for pressures of 19–61 GPa. This is lower than observed for four-coordinated silicates such as ringwoodite (t/G = ~5–7% in the pressure range of 6–27 GPa) (Kavner and Duffy, 2001a) and olivine (Uchida et al., 1995) but comparable to another six-coordinated silicate, stishovite and its $CaCl_2$-type modification (t/G = ~2–4% in the pressure ranges of 15–61 GPa) (Shieh et al., 2002). Therefore, these results support the previously observation (Shieh et al., 2002) that strength as a fraction of shear modulus for six-coordinated silicates is in general lower than that of four-coordinated silicates at high pressures. Similar results have been reported for silica glass using radial pressure gradient measurements in a diamond anvil cell (Meade and Jeanloz, 1990). It is also worth noting that the t/G values of $CaSiO_3$ perovskite are close to stishovite values, which may indicate a common behavior for octahedral silicates at high pressure. Our observations here can be compared to systematic relations for the normalized flow stress, σ/G, observed for different crystal structures of dense oxides in high-temperature

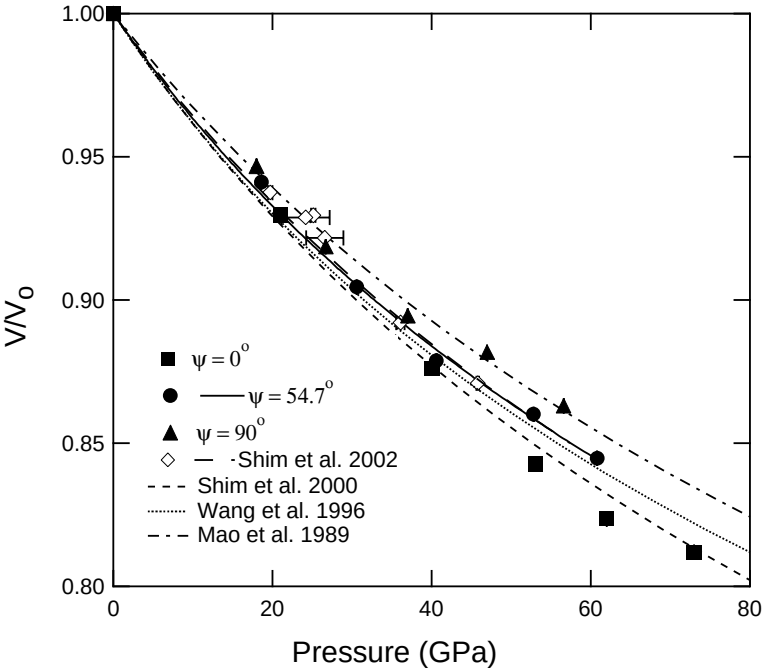

Fig. 4. Equation of state of $CaSiO_3$ perovskite at $\psi = 0$, 54.7, and 90°. Solid symbols are from this study and solid line is a fit to a third-order Birch-Manurghan equation of state. Open diamonds are from Shim et al. (2002) and long dash line is a fit to their data.

deformation experiments (Karato, 1989). In that study, the normalized flow stress was observed to decrease in the order spinel, olivine, and perovskite just as we observed in our low-temperature experiments (Fig. 5). A systematic dependence of yield strength on crystal structure, thus, appears to extend across high- and low-temperature deformation regimes. Further studies are needed, however, to confirm the structural trends observed in diamond cell experiments.

To obtain the differential stress supported by $CaSiO_3$ perovskite, it is necessary to know the shear modulus. While estimates of the shear modulus of $CaSiO_3$ perovskite have been made at ambient pressure based on elasticity systematics (Kung et al., 2001; Sinelnikov et al., 1998), there are no high-pressure experimental data available. However, the shear modulus for cubic $CaSiO_3$ has been determined by density functional theory calculations to pressures above 100 GPa (Karki and Crain, 1998). Using these values (and assuming $t = Y$), the yield strength of $CaSiO_3$ perovskite is found to increase from 3(1) GPa at 19 GPa to 11(1) GPa at 61 GPa (Fig. 6).

We find that six-coordinated silicates (e.g. $CaSiO_3$ perovskite and stishovite) support lower differential stresses than four-coordinated silicates even though the shear moduli of the six-coordinated silicates is larger. There have been several measurements of strength of orthorhombic perovskites with compositions at or near $(Mg_{0.9}Fe_{0.1})SiO_3$ (Meade and Jeanloz, 1990; Chen et al., 2002; Merkel et al., 2003) (Fig. 6). Meade and Jeanloz (1990) used measurements of pressure gradients across the sample to infer shear strengths which we converted to differential stress (yield strength) in Fig. 6. Merkel et al. (2003) used a similar technique as our study, and Chen et al. (2002) inferred the strength at room and high temperatures from measurements of diffraction peak linewidths in a multi-anvil press. For the data of Merkel et al. (2003) and Chen et al. (2002), the reported differential stresses for $(Mg_{0.9}Fe_{0.1})SiO_3$ are 2–3% of the shear modulus, consistent with our results for six-coordinated silicates. The strength of $(Mg_{0.9}Fe_{0.1})SiO_3$ perovskite is greater than $CaSiO_3$ perovskite. However, there remains considerable

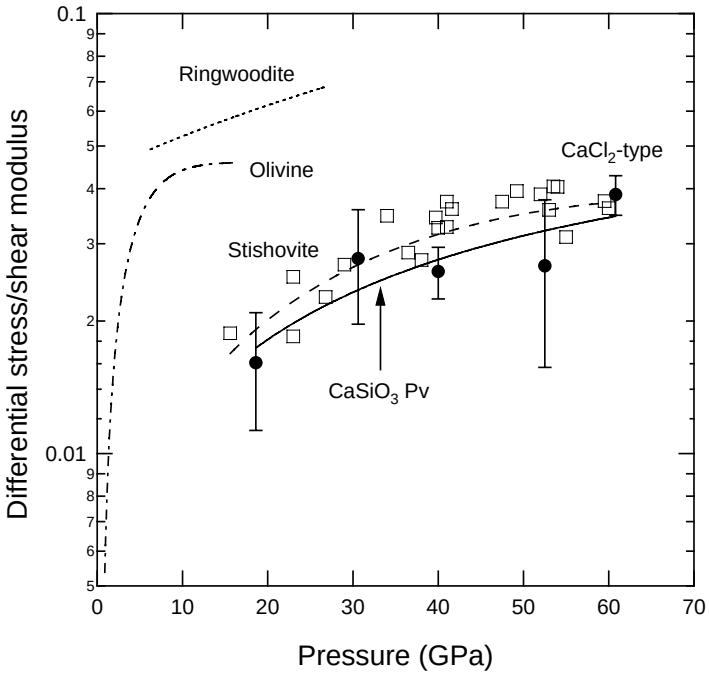

Fig. 5. The ratio of differential stress to shear modulus for $CaSiO_3$ perovskite (solid circles and line). Dotted line—ringwoodite (Kavner and Duffy, 2001a); dot-dashed line—olivine (Uchida et al., 1995); open squares and dashed line—SiO_2 (Shieh et al., 2002). The stishovite–$CaCl_2$-type phase boundary is near 50 GPa.

uncertainty in the strength of $(Mg_{0.9}Fe_{0.1})SiO_3$ as reported values vary by nearly a factor of 3 at 15–20 GPa. In high temperature experiments, it has been noted that the normalized creep strengths of perovskite compositions with orthorhombic symmetry are larger than those of compositions exhibiting cubic symmetry (Wang et al., 1999).

It is notable that lattice strain anisotropy and appreciable deviatoric stresses are observed at our lowest compression step (∼19 GPa) (Figs. 2 and 6) which was measured after laser heating but without further compression. It is generally believed that laser annealing greatly reduces or eliminates differential stresses in diamond cell samples. However, measurements of lattice strain anisotropy now allow the reduction in differential stress to be quantified. Our findings here are consistent with previous results from our laboratory (Shim et al., 2000; Kavner and Duffy, 2001b) which document significant residual differential stresses after laser heating. We note, however, that all these observations follow laser heating restricted to a single heated spot or a series of heated spots, rather than continuous rastering of the laser beam across the sample.

In cases where the elastic tensor is known, Eq. (2) can be solved for individual diffraction lines to investigate possible anisotropy of t (Eq. (4)). For the cubic crystal system, $G_R(h\,k\,l)$ can also be related to the Young's modulus, $E(h\,k\,l)$ in the direction normal to the diffraction plane, and the linear compressibility, β (Uchida et al., 1996)

$$\frac{1}{2G_R^X(hkl)} = \frac{1}{2}\left(\frac{3}{E(hkl)} - \beta\right) = S_{11} - S_{12} - 3S\Gamma(hkl). \quad (11)$$

The results for specific diffraction lines and converting compliances, S_{ij}, into elastic stiffnesses, C_{ij}, are

$$G_R^X(200) = \frac{1}{2}(C_{11} - C_{12}), \quad (12)$$

$$G_R^X(111) = C_{44}, \quad (13)$$

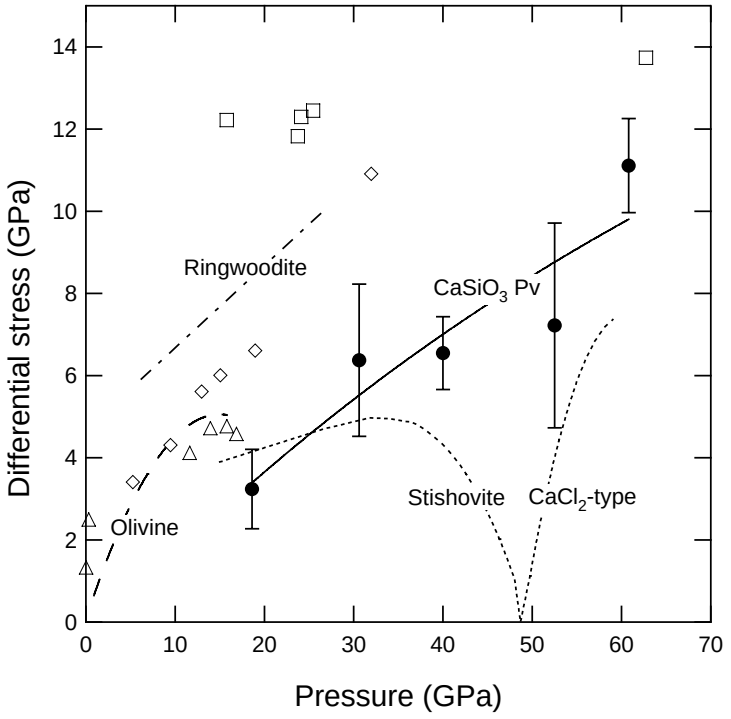

Fig. 6. The supported differential stress for $CaSiO_3$ perovskite using the (cubic) shear modulus of Karki and Crain (1998) (solid circles and line). The dash-dotted line denotes ringwoodite values (Kavner and Duffy, 2001a); dashed line denotes olivine values (Uchida et al., 1995); dotted line denotes SiO_2 values (stishovite to 50 GPa, $CaCl_2$-type structure at >50 GPa) (Shieh et al., 2002). Data for perovskite compositions close to $(Mg_{0.9}Fe_{0.1})SiO_3$ are shown as open squares (Meade and Jeanloz, 1990), open triangles (Chen et al., 2002), and open diamonds (Merkel et al., 2003).

$$G_R^X(211) = G_R^X(110) = \frac{4C_{44}}{A+3}. \quad (14)$$

Using the cubic elastic tensor results of Karki and Crain (1998), we find, for example at 41 GPa, $G_R(200) = 195$ GPa, $G_R(110) = G_R(211) = 266$ GPa, and $G_R(111) = 303$ GPa. Using these results in Eq. (4), we obtain the differential stresses, $t(hkl)$, shown in Fig. 7. While the (110), (220), (200), and (111) planes yield similar values, $t(hkl)$ corresponding to the (211) planes is larger at high pressure, as expected from Fig. 3. The high value of (211) relative to (110) is not affected by uncertainty in Reuss shear modulus for these planes as $G_R(211) = G_R(110)$. Our results suggest that strengths on the (100), (110), and (111) planes are similar in magnitude. This is similar to high-temperature observations on oxide perovskites in which slip is observed on $\langle 001\rangle\{100\}$, $\langle 110\rangle\{1\bar{1}0\}$, and $\langle 1\bar{1}0\rangle\{111\}$ systems (Beauchesne and Poirier, 1990). However, deformation experiments on oxide perovskites have revealed a wide range of creep laws, and it is not easy to generalize across compositions (Wright et al., 1992).

An alternative approach, and the way in which strain anisotropy data in the diamond anvil cell have been normally analyzed (e.g. Singh et al., 1998; Duffy et al., 1999; Merkel et al., 2002), is to assume no strength anisotropy and to directly invert for the elastic moduli (Eqs. (3), (5)–(7)). Again, we emphasize that the following results are dependent on the assumption that the slight tetragonal (or lower symmetry) distortion observed by Shim et al. (2002), but undetectable with the techniques of this study, do not affect the results of Fig. 2. This assumption will need to be tested in future work. In general, our single-crystal elastic constants for $CaSiO_3$ perovskite show good agreement with first-principles calculations (Karki

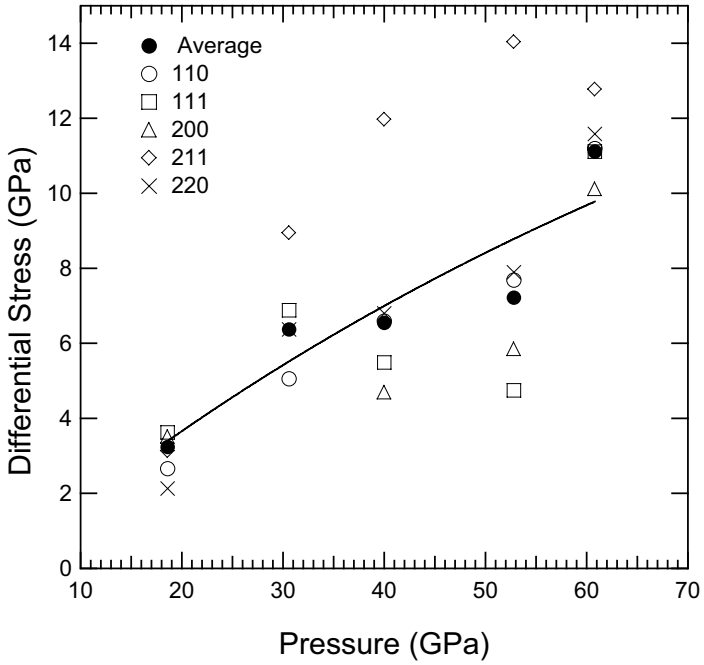

Fig. 7. The differential stress obtained from individual ($h\,k\,l$) reflections based on Eq. (4) (see text). The solid circles are data from the average value of $Q(h\,k\,l)$ based on Eq. (3).

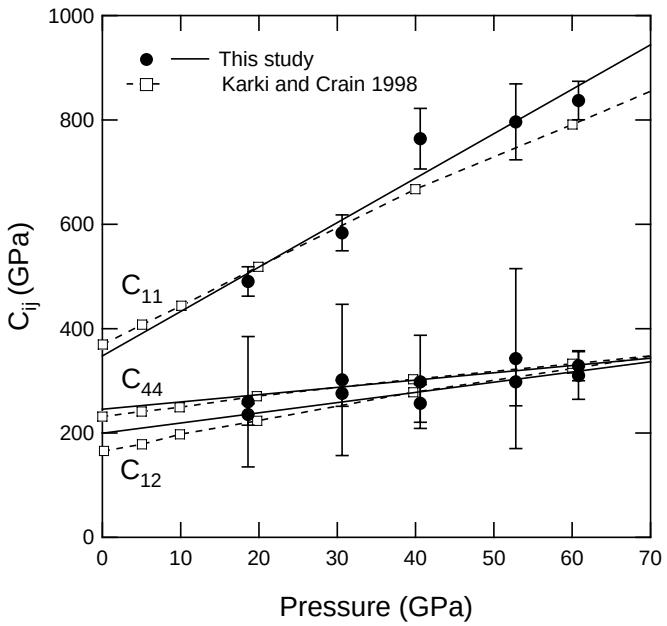

Fig. 8. The second-order cubic elastic constants of cubic $CaSiO_3$ perovskite as a function of pressure. Solid symbols and lines are from this study. Open squares and dashed lines are from Karki and Crain (1998).

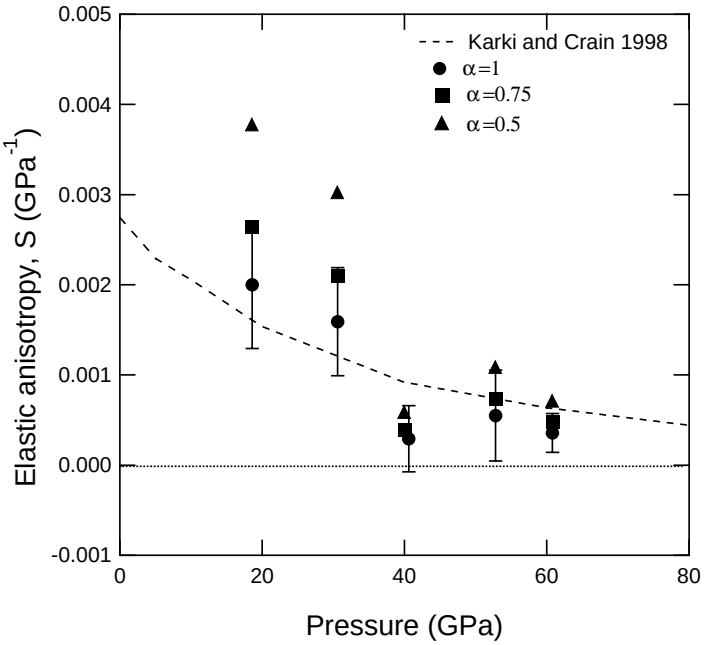

Fig. 9. Elastic anisotropy, *S*, as a function of pressure. The dashed line is from Karki and Crain (1998). For clarity, error bars are only shown for $\alpha = 1$.

and Crain, 1998) (Fig. 8). When we vary α, the parameter governing stress continuity, from 1 to 0.5, it is found that C_{11} decreases and C_{12} increases. For C_{44}, the values obtained at $\alpha = 0.5$ are much larger at low pressure but becomes close to those of the theoretical predication and values from $\alpha = 1$ at high pressure. The anisotropy factor, $S = S_{11} - S_{12} - 0.5S_{44}$, decreases with increasing pressure, from 0.0020(7) to 0.0004(2) GPa^{-1} when α is assumed to be 1 (Fig. 9). The observed trend is in general good accord with the theoretical predictions (Karki and Crain, 1998). When we reduce the value of α to 0.75 and 0.5, the elastic anisotropy increases by a more pronounced amount at low pressure. Furthermore, the anisotropy deviates increasingly from the theoretical results, suggesting that $\alpha \approx 1$ is appropriate for this experiment. In fact, we continue to observe a strong decrease in elastic anisotropy with pressure in all cases. Thus, a decrease in the elastic anisotropy of $CaSiO_3$ with pressure, consistent with theoretical predictions, is supported by our data, even in the case where α decreases with pressure.

4. Conclusion

Radial X-ray diffraction of $CaSiO_3$ perovskite under non-hydrostatic loading and assuming a pseudo-cubic structure yields a quasi-hydrostatic equation of state in good agreement with previous experiments. The ratio of differential stress to shear modulus, *t*/*G* varies between 2 and 4% in the pressure range of 19–61 GPa. This value is similar to that of stishovite and suggests a common behavior of six-coordinated silicates at mantle pressures. The differential stress or yield strength for $CaSiO_3$ perovskite increases from 3 to 11 GPa over the pressure range of our study. Direct inversion for the cubic elastic constants and elastic anisotropy of $CaSiO_3$ perovskite from lattice strains yields good agreement with theoretical predictions (Karki and Crain, 1998). However, there is evidence for possible strength anisotropy. Our results indicate the elastic anisotropy decreases with compression. While the recently discovered symmetry-reducing distortion of $CaSiO_3$ perovskite does not appear to measurably affect the angle dependence of lattice

strain, numerical values for t and the C_{ij} tensor depend on the assumption that the theoretically calculated shear modulus and measured lattice strain anisotropy are not drastically affected by this distortion. Future studies will be required to evaluate this assumption.

Acknowledgements

We thank N. Sata and V. Prakapenka for experimental assistance, and S. Speziale for helpful discussion. We also thank two anonymous reviewers for improving this work. This study was supported by NSF and the David and Lucille Packard Foundation.

References

Akber-Knutson, S., Bukowinski, M.S.T., Matas, J., 2002. On the structure and compressibility of $CaSiO_3$ perovskite. Geophys. Res. Lett. 29 (10.1039/2001GL013523).

Beauchesne, S., Poirier, J.P., 1990. In search of a systematics for the viscosity of perovskites-creep of potassium tantalate and niobate. Phys. Earth Planet. Int. 61, 182–198.

Chen, J., Weidner, D.J., Vaughan, M.T., 2002. The strength of $Mg_{0.9}Fe_{0.1}SiO_3$ at high pressure and high temperature. Nature 419, 824–826.

Chizmeshya, A.V.G., Wolf, G.H., McMillan, P.F., 1996. First-principle calculation of the equation of state, stability, and polar optic modes of $CaSiO_3$ perovskite. Geophys. Res. Lett. 23, 2725–2728.

Duffy, T.S., Shen, G., Heinz, D.L., Shu, J., Ma, Y., Mao, H.K., Hemley, R.J., Singh, A.K., 1999. Lattice strains in gold and rhenium under nonhydrostatic compression to 37 GPa. Phys. Rev. B 60, 15063–15073.

Evans, B., Goetze, C., 1979. Temperature-variation of hardness of olivine and its implication for polycrystalline yield stress. J. Geophys. Res. 84, 5505–5524.

Fiquet, G., 2001. Mineral phases of the Earth's mantle. Z. Kristallogr. 216, 248–271.

Hemley, R.J., Jackson, M.D., Gordon, R.G., 1987. Theoretical study of the structure, lattice dynamics, and equation of state of perovskite-type $MgSiO_3$ and $CaSiO_3$. Phys. Chem. Miner. 14, 2–12.

Holmes, N.C., Moriarty, J.A., Gathers, G.R., Nellis, W.J., 1989. The equation of state of platinum to 660 GPa (6.6 Mbar). J. Appl. Phys. 66, 2962–2967.

Joswig, W., Stachel, T., Harris, J.W., Baur, W.H., Brey, G.P., 1995. New Ca-silicate inclusion in diamonds—tracers from the lower mantle. Earth Planet. Sci. Lett. 173, 1–6.

Karato, S., 1989. Plasticity crystal-structure systematics in dense oxides and its implications for creep strength of the Earth's deep interior. Phys. Earth Planet. Int. 55, 234–240.

Karato, S., Fujuno, K., Ito, E., 1990. Plasticity of $MgSiO_3$ perovskite—the results of microhardness tests on single-crystals. Geophys. Res. Lett. 17, 13–16.

Karki, B.B., Crain, J., 1998. First-principle determination of elastic properties of $CaSiO_3$ perovskite at lower mantle pressure. Geophys. Res. Lett. 25, 2741–2744.

Kato, T., Ringwood, A.E., Irifune, T., 1988. Experimental-determination of element partitioning between silicate perovskites, garnets and liquids-constrains on early differentiation of the mantle. Earth Planet. Sci. Lett. 89, 123–145.

Kavner, A., Duffy, T.S., 2001a. Strength and elasticity of ringwoodite at upper mantle pressure. Geophys. Res. Lett. 28, 2691–2694.

Kavner, A., Duffy, T.S., 2001b. Pressure–volume–temperature paths in the laser-heated diamond anvil cell. J. Appl. Phys. 89, 1907–1914.

Kumazawa, M., 1969. Elastic constant of polycrystalline rocks and nonelastic behavior inherent to them. J. Geophys. Res. 74, 5311–5320.

Kung, J., Angel, R.J., Ross, N.L., 2001. Elasticity of $CaSnO_3$ perovskite. Phys. Chem. Miner. 28, 35–43.

Magyari-Köpe, B., Vitos, L., Grimvall, G., Jonason, B., Kollar, J., 2002. Low-temperature crystal structure of $CaSiO_3$ perovskite: an ab initial total energy study. Phys. Rev. B 65, 193107.

Mao, H.K., Chen, L.C., Hemley, R.J., Jephcoat, A.P., Wu, Y., Bassett, W.A., 1989. Stability and equation of state of $CaSiO_3$ perovskite to 134 GPa. J. Geophys. Res. 94, 17889–17894.

Meade, C., Jeanloz, R., 1990. The strength of mantle silicates at high pressures and room temperature: implications for the viscosity of the mantle. Nature 348, 533–535.

Merkel, S., Badro, J., Montagnac, G., Gillet, P., Mao, H.K., Hemley, R.J., 2003. Deformation of $(Mg_{0.9}, Fe_{0.1})SiO_3$ perovskite aggregates up to 32 GPa. Earth Planet. Sci. Lett. 209, 351–360.

Merkel, S., Jephcoat, A.P., Shu, J., Mao, H.K., Gillet, P., Hemley, R.J., 2002. Equation of state, elasticity, and shear strength of pyrite under high pressure. Phys. Chem. Miner. 29, 1–9.

Shen, G., River, M.L., Wang, Y., Sutton, S.R., 2001. Laser heated diamond cell system at the advanced photon source for in situ X-ray measurements at high pressure and temperature. Rev. Sci. Instrum. 72, 1273–1282.

Sherman, D.M., 1993. Equation of state, elastic properties, and stability of $CaSiO_3$ perovskite—first-principles (periodic Hartree-Fock) results. J. Geophys. Res. 98, 19795–19805.

Shieh, S.R., Duffy, T.S., Li, B., 2002. Strength and elasticity of stishovite across the stishovite-$CaCl_2$-type structural phase boundary. Phys. Rev. Lett. 89, 255507.

Shim, S.H., Duffy, T.S., Kenichi, T., 2002. Equation of state of gold and its application to the phase boundaries near 660 km depth in Earth's mantle. Earth Planet. Sci. Lett. 203, 729–739.

Shim, S.H., Duffy, T.S., Shen, G., 2000. The equation of state of $CaSiO_3$ perovskite to 108 GPa at 300 K. Phys. Earth Planet. Int. 120, 327–338.

Shim, S.H., Duffy, T.S., Shen, G., 2000. The stability and P–V–T equation of state of $CaSiO_3$ perovskite in the Earth's lower mantle. J. Geophys. Res. 105, 25955–25968.

Shim, S.H., Jeanloz, R., Duffy, T.S., 2002. Tetragonal structure of $CaSiO_3$ perovskite above 20 GPa. Geophys. Res. Lett. 29 (10.1029/2002GL016148).

Sinelnikov, Y.D., Chen, G., Liebermann, R.C., 1998. Elasticity of $CaTiO_3$–$CaSiO_3$ perovskites. Phys. Chem. Miner. 25, 515–521.

Singh, A.K., 1993. The lattice strain in a specimen (cubic system) compressed nonhydrostatically in an opposed anvil device. J. Apply. Phys. 73, 4278–4286.

Singh, A.K., Balasingh, C., Mao, H.K., Hemley, R.J., Shu, J., 1998. Analysis of lattice strains measured under nonhydrostatic pressure. J. Appl. Phys. 83, 7567–7575.

Stixrude, L., Cohen, R.E., Yu, R., Krakauer, H., 1996. Prediction of phase transition in $CaSiO_3$ perovskite and implications for lower mantle structure. Am. Mineral. 81, 1293–1296.

Uchida, T., Funamori, N., Ohtani, T., Yagi, T., 1995. Differential stress of MgO and Mg_2SiO_4 under uniaxial stress field: variation with pressure, temperature, and phase transition, in: Proceedings of the 15th AIPAPT Conference, Warsaw, 1995, pp. 183–185.

Uchida, T., Funamori, N., Yagi, T., 1996. Lattice strains in crystals under uniaxial stress field. J. Appl. Phys. 80, 739–746.

Wang, Y., Weidner, D.J., Guyot, F., 1996. Thermal equation of state of $CaSiO_3$ perovskite. J. Geophys. Res. 101, 661–672.

Wang, Z., Dupas-Bruzek, C., Karato, S., 1999. High temperature creep of an orthorhombic perovskite-$YAlO_3$. Phys. Earth Planet. Int. 110, 51–69.

Wentzcovitch, R., Ross, N.L., Price, G.D., 1995. Ab initial study of $MgSiO_3$ and $CaSiO_3$ perovskites at lower-mantle pressures. Phys. Earth Planet. Int. 90, 101–112.

Wright, K., Price, D.C., Poirier, J.P., 1992. High-temperature creep of the perovskites $CaTiO_3$ and $NaNbO_3$. Phys. Earth Planet. Int. 74, 9–22.